



Citation for published version:

Daniels, E, Mustafa, Y, Herdes, C & Leese, H 2021, 'Optimization of Cortisol-Selective Molecularly Imprinted Polymers Enabled by Molecular Dynamics Simulations', *ACS Applied Bio Materials*, vol. 4, no. 9, pp. 7243-7253. <https://doi.org/10.1021/acsabm.1c00774>

DOI:

[10.1021/acsabm.1c00774](https://doi.org/10.1021/acsabm.1c00774)

Publication date:

2021

Document Version

Peer reviewed version

[Link to publication](https://doi.org/10.1021/acsabm.1c00774)

This document is the Accepted Manuscript version of a Published Work that appeared in final form in *ACS Applied Biomaterials*, copyright © American Chemical Society after peer review and technical editing by the publisher. To access the final edited and published work see <https://doi.org/10.1021/acsabm.1c00774>

University of Bath

Alternative formats

If you require this document in an alternative format, please contact:
openaccess@bath.ac.uk

General rights

Copyright and moral rights for the publications made accessible in the public portal are retained by the authors and/or other copyright owners and it is a condition of accessing publications that users recognise and abide by the legal requirements associated with these rights.

Take down policy

If you believe that this document breaches copyright please contact us providing details, and we will remove access to the work immediately and investigate your claim.

Supporting Information: Optimization of cortisol-selective molecularly imprinted polymers enabled by molecular dynamics simulations

Emma Daniels^{a,b,†}, Yasemin L. Mustafa^{b,d,†}, Carmelo Herdes^{c,*} and Hannah S. Leese^{a,b,c,d,*}

^a Centre for Sustainable Circular Technologies (CSCT), Department of Chemistry, University of Bath, Bath, BA2 7AY, UK.

^b Materials for Health Lab, Department of Chemical Engineering, University of Bath, Bath, BA2 7AY, UK.

^c Centre for Advanced Separations Engineering (CASE), University of Bath, Bath, BA2 7AY, UK.

^d Centre for Biosensors, Bioelectronics and Biodevices (C3Bio), University of Bath, Bath, BA2 7AY, UK.

[†]contributed equally. *Corresponding authors h.s.leese@bath.ac.uk, cehm21@bath.ac.uk

Table of Contents

Figure S1. UV/Vis analysis of successive washings with methanol. The specific absorption of cortisol at 242 nm has been highlighted.

Figure S2. Calibration curve for the cortisol concentrations of 0.2, 0.4, 0.6, 0.8, and 1.0 μM , respectively.

Figure S3. Illustration of i) cortisol captured by MIP during the rebinding experiments and ii) collection of captured cortisol by washing column with anhydrous methanol. Created with [BioRender.com](https://www.biorender.com).

Figure S4. Simulated (dotted line) and experimental (solid line) vapor-liquid equilibria of pure **a**) dichloromethane and **b**) methanol.

Figure S5. Optical microscope images of milled NIP particles used in particle size determination.

Figure S6. Optical microscope images of milled MIP particles used in particle size determination.

Figure S7. FE-SEM images of NIP particles at (a) 1,000 and (b) 50,000 magnification. Corresponding images of MIP particles at (c) 1,000 and (d) 50,000 magnification.

Figure S8. TGA of a) MIP and b) NIP heated from 25 to 650 $^{\circ}\text{C}$ under Argon at a rate of 10 $^{\circ}\text{C}/\text{min}$.

Figure S9. DSC of a) NIP powder and b) MIP powder: first heating cycle ran from -80 to 200 $^{\circ}\text{C}$ under nitrogen at a rate of 10 $^{\circ}\text{C}/\text{min}$. Second heating cycle ran from -80 to 500 $^{\circ}\text{C}$ at a rate of 10 $^{\circ}\text{C}/\text{min}$.

Figure S10. Mass spectrometry data obtained during TGA analysis of a) NIP particles and b) MIP particles plotted as experiment duration against the mass charge ratio of detected fragments. The plot colours indicate the relative intensity of each detected. The time at which the TGA furnace reaches 100 $^{\circ}\text{C}$ has been indicated.

Figure S11. Estimated volume of a single cortisol molecule using an ellipsoid model.

Figure S12. N_2 adsorption measurements of a) the CL9 MIP and b) the CL30 NIP and MIP formulations CL9/18/24/30.

Figure S13. Total energy evolution for CL9 system for the production cell – equilibration time around 600 ps.

Figure S14. RDF comparison plots, $g(r)$ vs r between the centre of mass interactions MAA-CTS and EGDMA-CTS for each model system CL9-CL60.

Figure S15.(A-F) include the RDF plot, $g(r)$ vs r , the repulsive (negative-grey) and attractive (positive-orange) regions ($(g(r)-1)r^2$ vs r) and the KBI vs r for the centre of mass (COM) interactions MAA-CTS and EGDMA-CTS for each model system CL9-CL60.

Figure S16. RDFs comparison plots between the atom pairs of MAA-CTS and EGDMA-CTS for each model system CL9-CL60.

Figure S17. KBI comparison plots between the atom pairs of MAA-CTS and EGDMA-CTS for each model system CL9-CL60.

Figure S18(A-F). include the repulsive (negative-grey) and attractive (positive-orange) filled regions ($(g(r)-1)r^2$ vs r) for the atom pairs labelled in **Figure 4** for MAA-CTS and EGDMA-CTS for each model system CL9-CL60.

Table S1. MIP and NIP surface area calculated using the Brunauer-Emmett-Teller (BET) theory, obtained using an Autosorb-iQ-C machine by Quantachrome Anton Paar, and the ASiQWin programme. CL30* in Entry 5 indicates a repeat using material from a second batch of synthesis. The NIP (Entry 6) here is based on the CL30 system.

Table S2. MIP and NIP pore size distributions calculated using the Barrett-Joyner-Halenda (BJH) analysis, obtained using an Autosorb-iQ-C machine by Quantachrome Anton Paar, and the ASiQWin programme. CL30* in Entry 5 indicates a repeat using material from a second batch of synthesis. The NIP (Entry 6) here is based on the CL30 system.

Table S3. Equilibration times for production cells per system – averages were taken discarding these times.

Table S4. The maximum RDF peaks, $g(r)$ max, and the distance at which the maximum occurs, $r_{(g(r)\text{max})}$, between the centre of mass of molecule pairs within each model system.

Table S5. The maximum RDF peaks, $g(r)$ max, distance at which the maximum occurs, $r_{(g(r)\text{max})}$, for specific interactions between atom i of cortisol and atom j of MAA and EGDMA within the CL9-60 modelled systems.

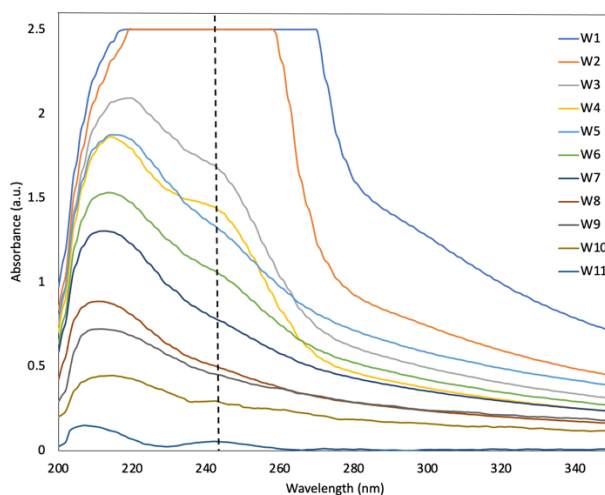


Figure S1. UV/Vis analysis of successive washings with methanol. The specific absorption of cortisol at 242 nm has been highlighted.

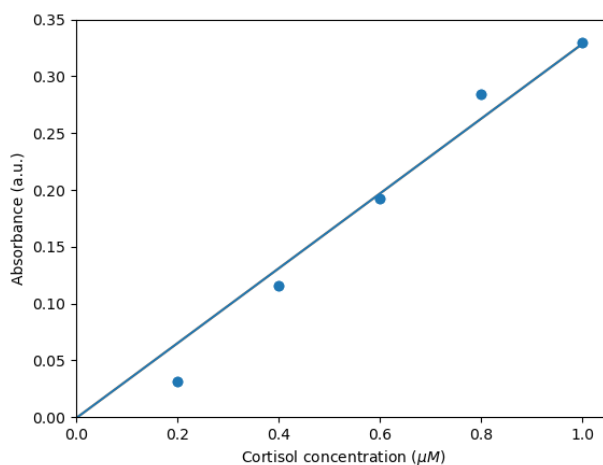


Figure S2. Calibration curve for the cortisol concentrations of 0.2, 0.4, 0.6, 0.8, and 1.0 μM , respectively.

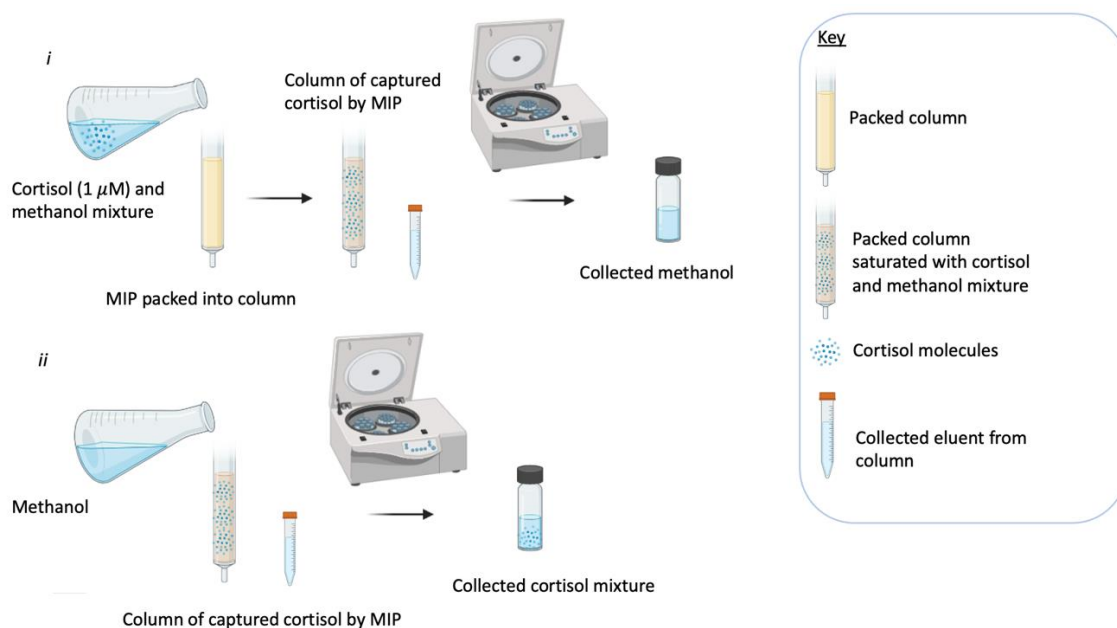
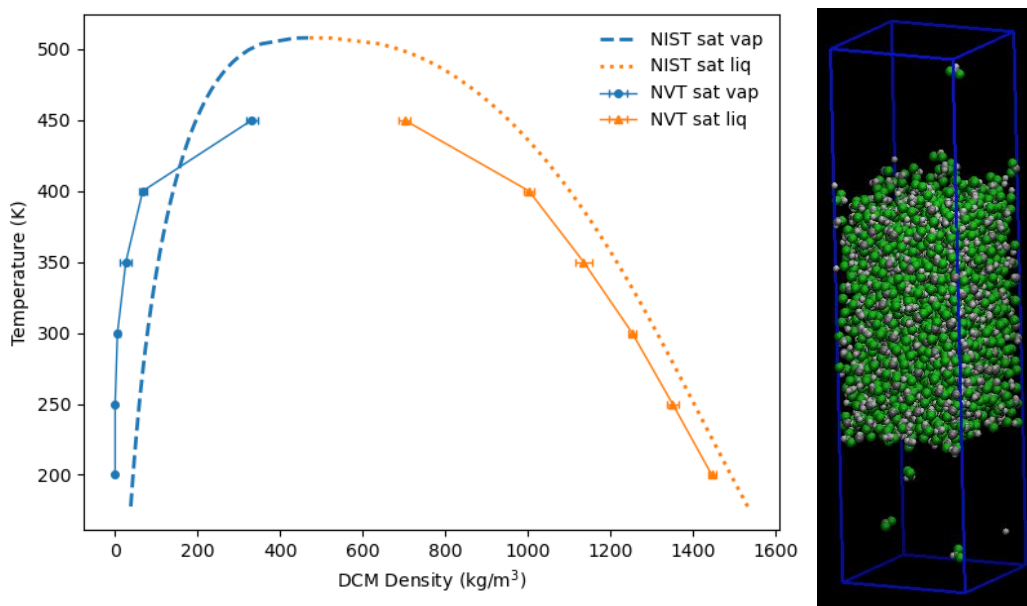


Figure S3. Illustration of i) cortisol captured by MIP during the rebinding experiments and ii) collection of the captured cortisol by washing column with anhydrous methanol. Created with [BioRender.com](https://www.biorender.com).

Validation of Solvent Models

NVT simulation results for the vapour-liquid equilibria for pure DCM, and methanol are compared to experimental data from the NIST Chemistry Webbook (<https://webbook.nist.gov/chemistry/>). An elongated simulation box allows the coexistence of the two phases in the needed temperature range, average densities were calculated at the bulk of each phase after equilibration.

a)



b)

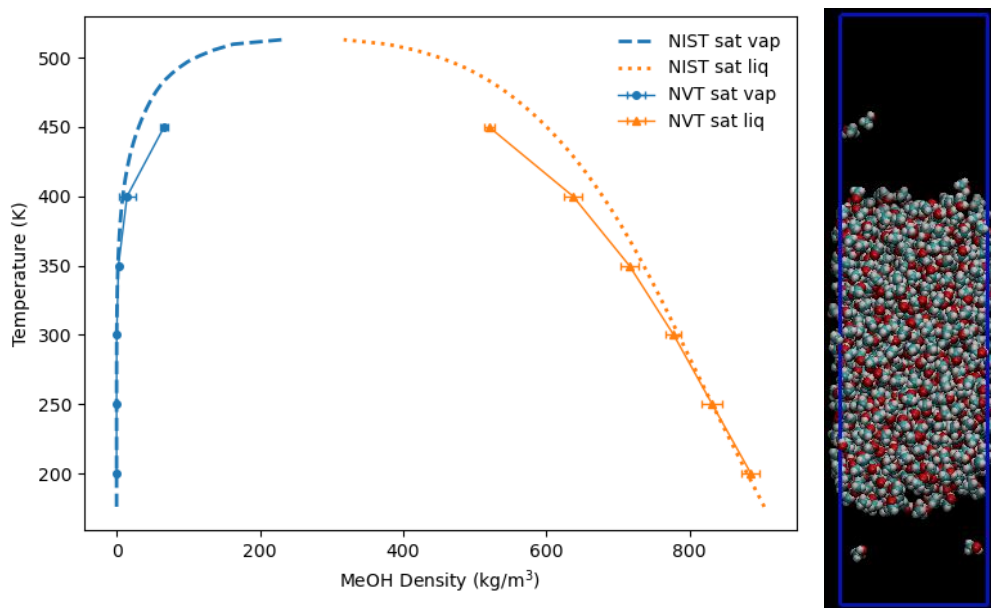


Figure S4. Simulated (dotted line) and experimental (solid line) vapor-liquid equilibria of pure **a)** dichloromethane and **b)** methanol.

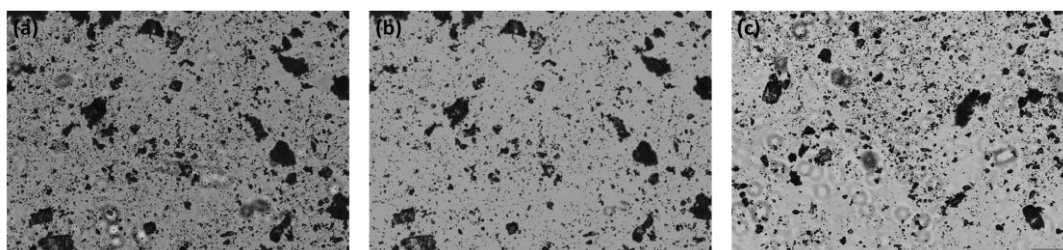


Figure S5 Optical microscope images of milled NIP particles (a-c) used in particle size determination.

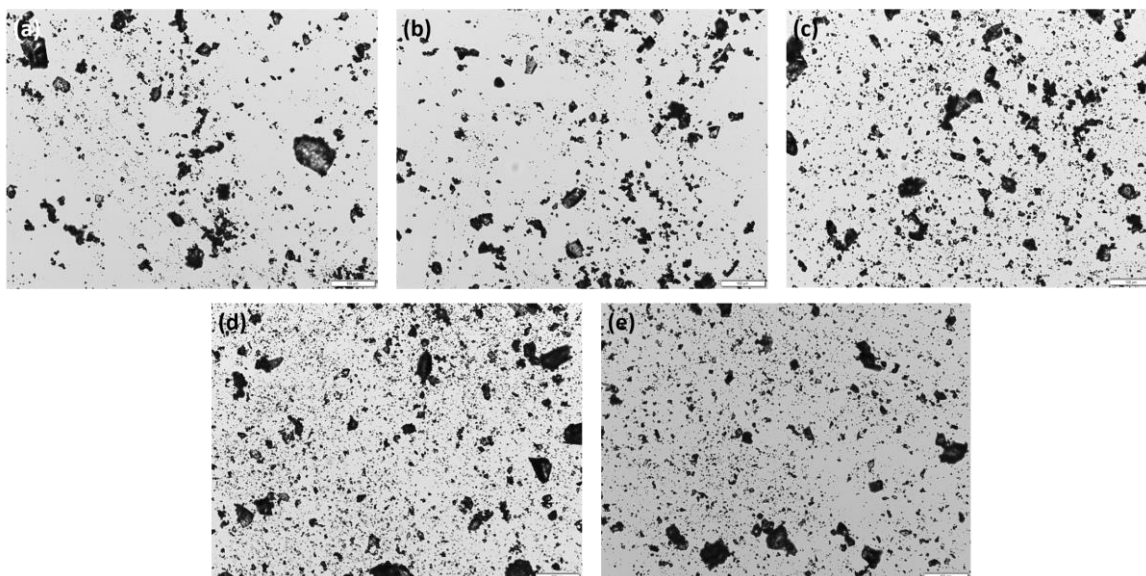


Figure S6. Optical microscope images of milled MIP particles (a-e) used in particle size determination.

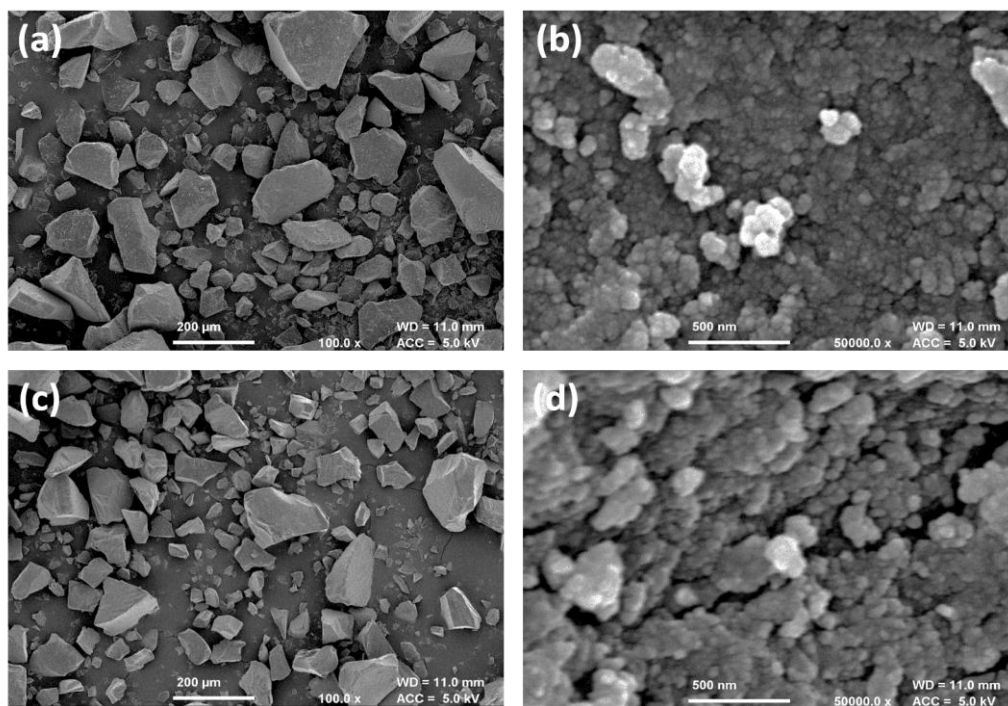
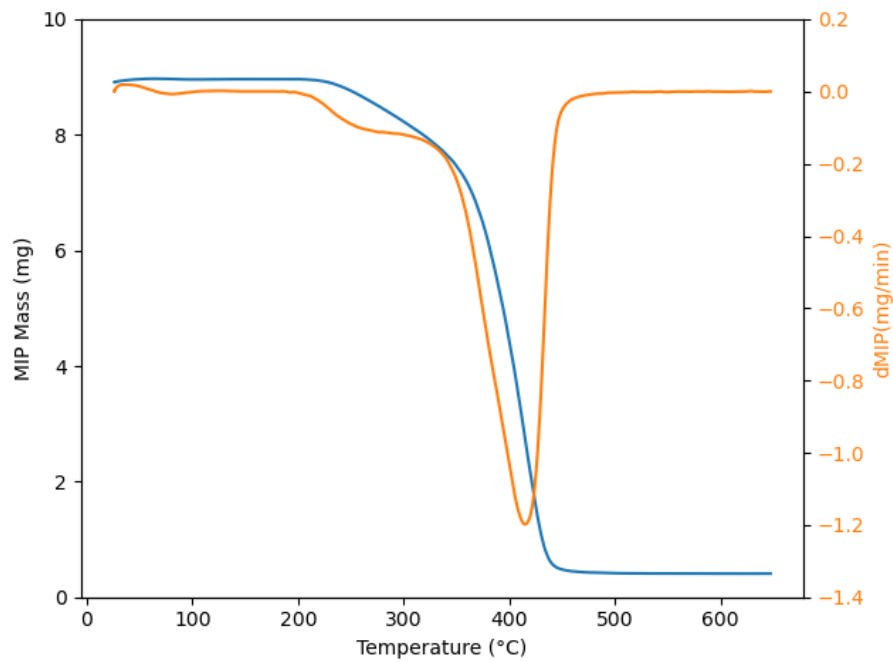


Figure S7. FE-SEM images of NIP particles at (a) 1,000 and (b) 50,000 magnification. Corresponding images of MIP particles at (c) 1,000 and (d) 50,000 magnification.

a)



b)

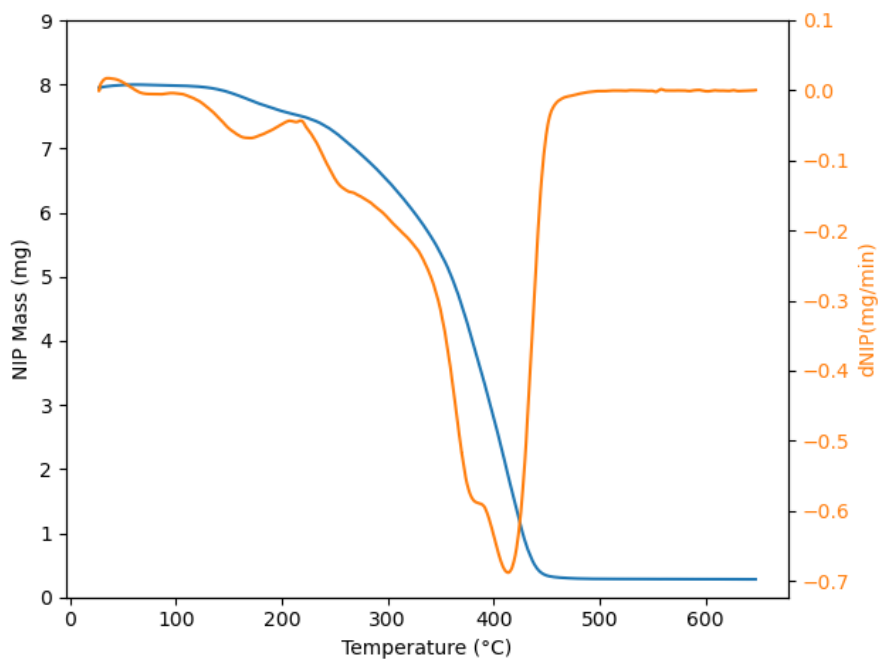


Figure S8. TGA of a) MIP and b) NIP heated from 25 to 650 °C under Argon at a rate of 10 °C /min.

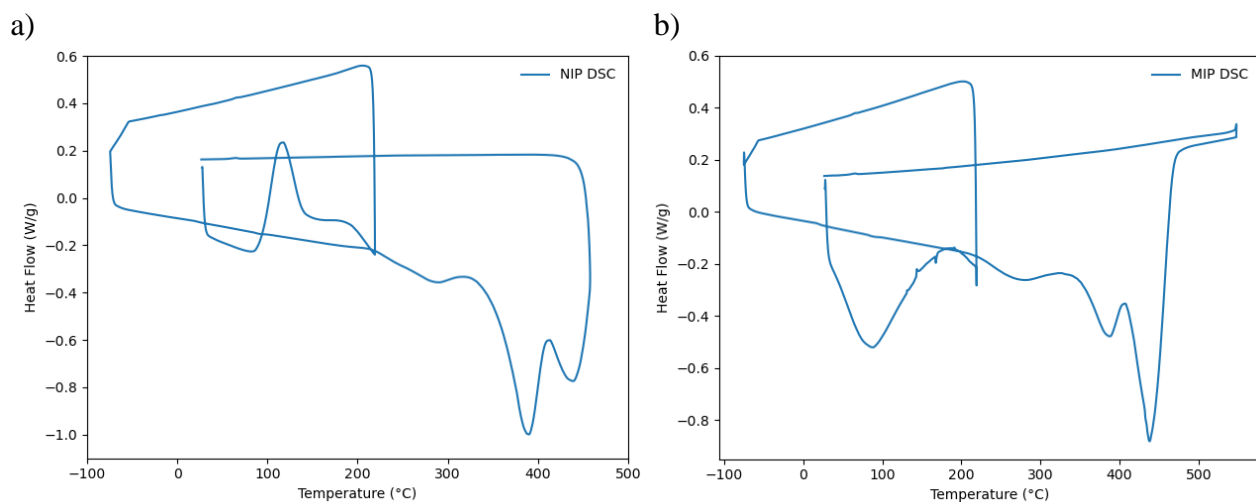


Figure S9. DSC of a) NIP powder and b) MIP powder: first heating cycle ran from 25 to 200 °C under nitrogen at a rate of 10 °C /min. Second heating cycle ran from -80 to 500 °C at a rate of 10 °C /min., before cooling to 25 °C.

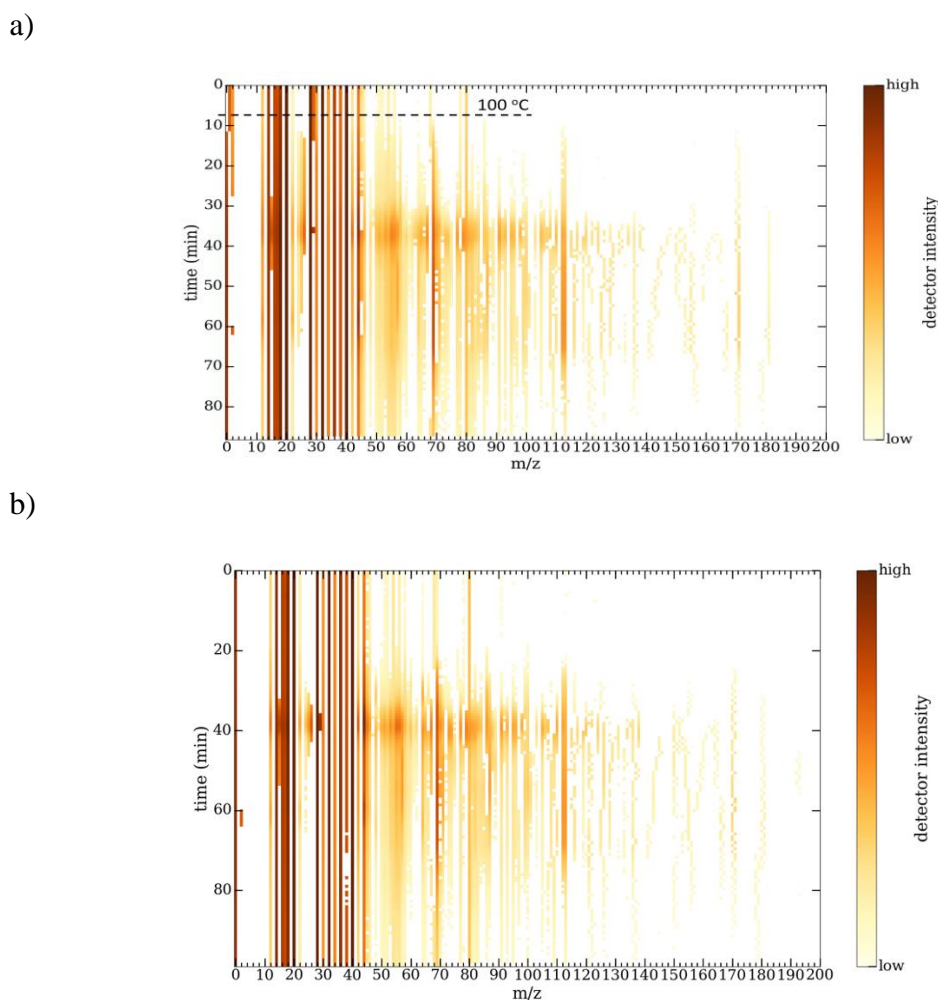


Figure S10. Mass spectrometry data obtained during TGA analysis of a) NIP particles and b) MIP particles plotted as experiment duration against the mass charge ratio of detected fragments. The plot colours indicate the relative intensity of each detected. The time at which the TGA furnace reaches 100 °C has been indicated.

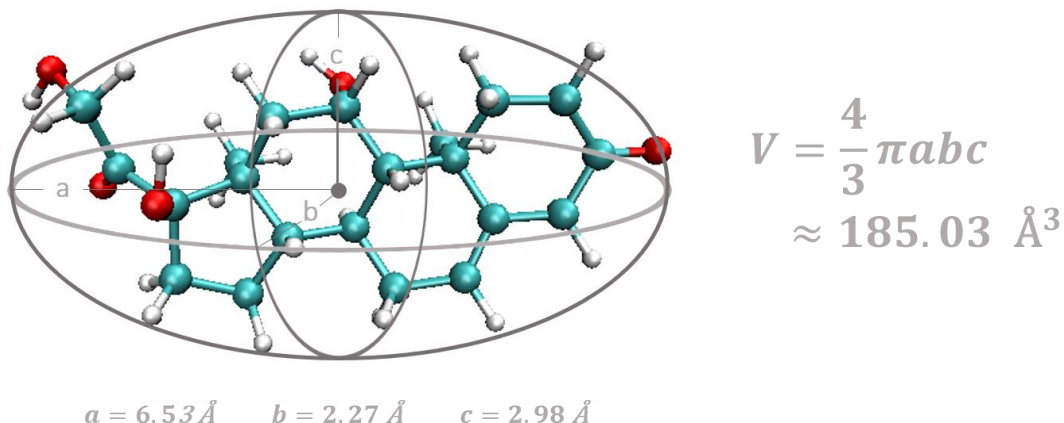


Figure S11. Estimated volume of a single cortisol molecule using an ellipsoid model.

BET Surface Area and BJH Pore Size Distribution Analysis

The surface area and pore size distribution analysis presented in the main body of this paper were conducted on a 3Flex machine from Micromeritics and calculations were performed within the MicroActive program. Samples were loaded into 12 mm wide glass tubes and degassed in situ with the aid of a heating chamber set at 100 °C. Adsorption of nitrogen was conducted at 77 K.

Due to decommission of the 3Flex during manuscript preparation, the results displayed below were obtained using an Autosorb-iQ-C machine by Quantachrome Anton Paar, with the data acquisition and processing program ASiQWin. Samples were inserted in a 9-mm glass tube (inner diameter) and degassed at room temperature for 10 hours. For the analysis, a glass rod was inserted in the tube in order to minimise the empty space. The N₂ adsorption isotherm was measured at 77 K in a liquid nitrogen bath. From the adsorption isotherm the BET surface area and the BJH pore size distributions were calculated.

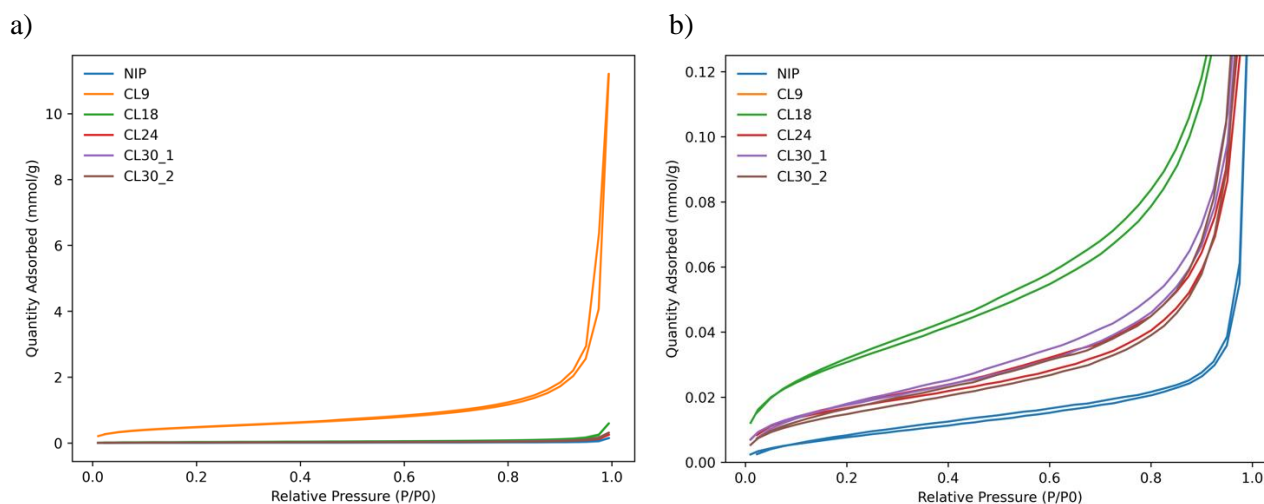


Figure S12. N₂ adsorption measurements of a) the CL9 MIP and b) the CL30 NIP and MIP formulations CL9/18/24/30.

Table S1. MIP and NIP surface area calculated using the Brunauer-Emmett-Teller (BET) theory, obtained using an Autosorb-iQ-C machine by Quantachrome Anton Paar, and the ASiQWin programme. CL30* in Entry 5 indicates a repeat using material from a second batch of synthesis. The NIP (Entry 6) here is based on the CL30 system.

Entry	System	Mass (g)	BET Surface Area (m ² /g)		
			1	2	3
1	CL30	0.4234	1.524	1.469	1.501
2	CL9	0.3503	38.384	38.288	39.268
3	CL18	0.5112	2.486	2.505	2.621
4	CL24	0.5250	1.436	1.475	1.381
5	CL30*	0.3871	1.375	1.342	1.292
6	NIP	0.5305	0.685	0.664	0.746

Table S2. MIP and NIP pore size distributions calculated using the Barrett-Joyner-Halenda (BJH) analysis, obtained using an Autosorb-iQ-C machine by Quantachrome Anton Paar, and the ASiQWin programme. CL30* in Entry 5 indicates a repeat using material from a second batch of synthesis. The NIP (Entry 6) here is based on the CL30 system.

Entry	System	Surface Area (m ² /g)	Pore Volume (cc/g)	Pore Diameter Dv(d) (nm)
1	CL30	1.204	0.011	1.573
2	CL9	29.803	0.384	3.316
3	CL18	2.038	0.020	2.981
4	CL24	0.995	0.009	1.574
5	CL30*	1.042	0.011	3.151
6	NIP	0.538	0.005	1.623

Additional Computational Methodology

To model the pre-polymerization mixtures, one cortisol molecule was added to a 6 nm cubic simulation box, the so-called unit cell. All other components of the pre-polymerization mixture (MAA, EGDMA, MeOH and DCM) were then added in the correct ratios relative to one cortisol molecule for each system. The systems were first subjected to NVT simulations with time steps of 0.1 fs for 1 ns and then compressed under NpT simulations at 10 bar until liquid densities were achieved, around 2 ns. After compression, the systems were allowed to equilibrate under NVT for 7 ns. The systems were then scaled up so that each production cell contained 192 cortisol molecules - using the *gmx genconf* command within GROMACS. Production runs under NVT ensembles were then performed on the larger systems for 7 ns with 1 fs time steps. When necessary, simulations were extended using the inbuilt *gmx convert-tpr* command within GROMACS. See flowchart in next page, and GROMACS .mdp files examples. Equilibration times shown in Table S3, where obtained from total energy evolution plots like Figure S13.

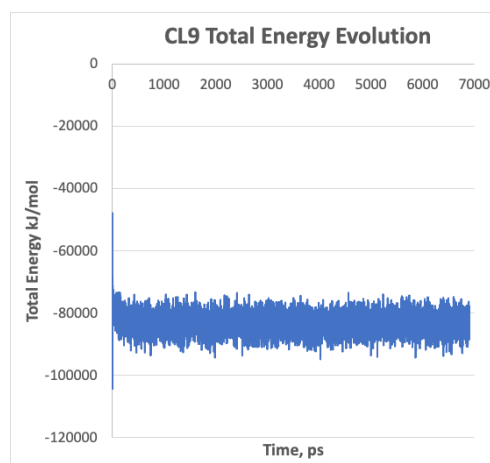
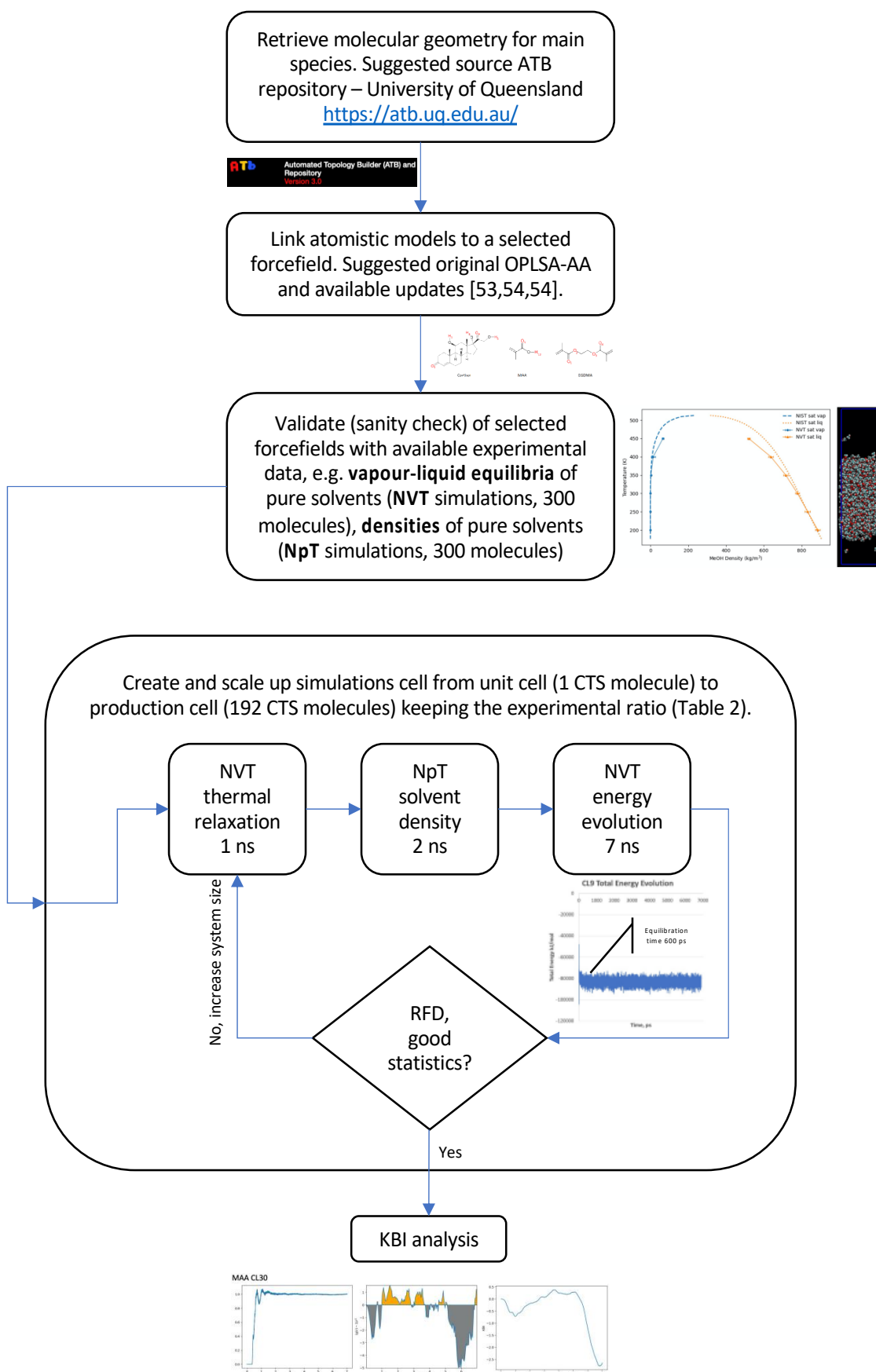


Figure S13. Total energy evolution for CL9 system for the production cell – equilibration time around 600 ps.

Table S3. Equilibration times for production cells per system – averages were taken discarding these times.

System	Equilibration time (ps)	System	Equilibration time (ps)
CL9	600	CL30	50
CL18	100	CL42	100
CL24	100	CL60	50



1_NVT mdp

```
constraints      = h-bonds
unconstrained-start=no
integrator       = md
dt              = 0.0001
tinit           = 0.0
nsteps          = 1000000
nstcomm         = 50000
nstxout         = 50000
nstvout         = 50000
nstxtcout       = 50000
xtc_precision   = 50000
nstfout         = 0
nstlog          = 10000
nstenergy       = 10000
nstlist         = 10
ns_type         = grid
coulombtype     = pme
cutoff-scheme   = Verlet
rlist           = 1.5
rcoulomb        = 1.5
rvdw            = 1.5
fourierspacing = 0.15
pme_order       = 6
ewald_rtol      = 1.E-5
optimize_fft    = yes
; Nose-hoover thermostat is ON for both groups
Tcoupl          = berendsen
tc-grps         = system
tau_t           = 0.2
ref_t           = 277.15
; Energy monitoring
energygrps     =
; Isotropic pressure coupling is now off
Pcoupl         = no
Pcoupltype     = isotropic
tau_p          = 0.2
compressibility = 4.5e-5
ref_p          = 1
; Generate velocities is on at 300 K.
gen_vel        = no
gen_temp       = 277.15
gen_seed       = 89713
pbc = xyz
;Have a nice simulation!
```

2_NpT Compression mdp

```
constraints      = h-bonds
unconstrained-start=no
integrator       = md
dt              = 0.0001
tinit           = 0.0
nsteps          = 5000000
nstcomm         = 50000
nstxout         = 50000
```

```

nstvout      = 50000
nstxtcout   = 50000
xtc_precision = 50000
nstfout     = 0
nstlog      = 10000
nstenergy   = 10000
nstlist     = 10
ns_type     = grid
coulombtype = pme
cutoff-scheme = Verlet
rlist       = 1.5
rcoulomb    = 1.5
rvdw        = 1.5
fourierspacing = 0.15
pme_order   = 6
ewald_rtol  = 1.E-5
optimize_fft = yes
; Nose-hoover thermostat is ON for both groups
Tcoupl      = berendsen
tc-grps     = system
tau_t       = 0.2
ref_t       = 277.15
; Energy monitoring
energygrps  =
; Isotropic pressure coupling is now off
Pcoupl      = berendsen
Pcoupltype  = isotropic
tau_p       = 0.2
compressibility = 4.5e-5
ref_p       = 10
; Generate velocities is on at 300 K.
gen_vel     = no
gen_temp    = 277.15
gen_seed    = 89713
pbc = xyz
;Have a nice simulation!

```

3_NpT mdp

```

constraints = h-bonds
unconstrained-start=no
integrator  = md
dt          = 0.001
tinit      = 0.0
nsteps     = 1000000
nstcomm    = 50000
nstxout    = 50000
nstvout    = 50000
nstxtcout  = 50000
xtc_precision = 50000
nstfout    = 0
nstlog     = 10000
nstenergy  = 10000
nstlist    = 10
ns_type    = grid
coulombtype = pme

```

```

cutoff-scheme = Verlet
rlist = 1.5
rcoulomb = 1.5
rvdw = 1.5
fourierspacing = 0.15
pme_order = 6
ewald_rtol = 1.E-5
optimize_fft = yes
; Nose-hoover thermostat is ON for both groups
Tcoupl = berendsen
tc-grps = system
tau_t = 0.2
ref_t = 277.15
; Energy monitoring
energygrps =
; Isotropic pressure coupling is now off
Pcoupl = berendsen
Pcoupltype = isotropic
tau_p = 0.2
compressibility = 4.5e-5
ref_p = 1.00
; Generate velocities is on at 300 K.
gen_vel = no
gen_temp = 277.15
gen_seed = 89713
pbc = xyz
;Have a nice simulation!

```

4_prod_NVT mdp

```

constraints = h-bonds
unconstrained-start=no
integrator = md
dt = 0.001
tinit = 0.0
nsteps = 2000000
nstcomm = 50000
nstxout = 50000
nstvout = 50000
nstxtcout = 50000
xtc_precision = 50000
nstfout = 0
nstlog = 10000
nstenergy = 10000
nstlist = 10
ns_type = grid
coulombtype = pme
cutoff-scheme = Verlet
rlist = 1.5
rcoulomb = 1.5
rvdw = 1.5
fourierspacing = 0.15
pme_order = 6
ewald_rtol = 1.E-5
optimize_fft = yes
; Nose-hoover thermostat is ON for both groups

```

```
Tcoupl      = berendsen
tc-grps     = system
tau_t       = 0.2
ref_t       = 277.15
; Energy monitoring
energygrps  =
; Isotropic pressure coupling is now off
Pcoupl      = no
Pcoupltype  = isotropic
tau_p       = 0.2
compressibility = 4.5e-5
ref_p       = 1.00
; Generate velocities is on at 300 K.
gen_vel     = no
gen_temp    = 277.15
gen_seed    = 89713
pbc = xyz
;Have a nice simulation!
```


Table S4. The maximum RDF peaks, $g(r)$ max, and the distance at which the maximum occurs, $r_{(g(r)\max)}$, between the centre of mass of molecule pairs within each model system.

	CL9		CL18		CL24		CL30		CL42		CL60	
	$g(r)_{\max}$	$r_{(g(r)\max)}$ (nm)	$g(r)_{\max}$	$r_{(g(r)\max)}$ (nm)	$g(r)_{\max}$	$r_{(g(r)\max)}$ (nm)	$g(r)_{\max}$	$r_{(g(r)\max)}$ (nm)	$g(r)_{\max}$	$r_{(g(r)\max)}$ (nm)	$g(r)_{\max}$	$r_{(g(r)\max)}$ (nm)
CTS-MAA	1.041	1.388	1.018	1.392	1.029	1.088	1.075	1.116	1.031	1.422	1.030	1.075
CTS-EGDMA	1.045	1.076	1.044	1.078	1.053	1.064	1.052	1.032	1.060	0.898	1.076	0.892
CTS-DCM	1.010	0.858	1.015	0.876	1.017	0.848	1.014	0.838	1.006	0.836	1.029	0.848
CTS-MeOH	1.010	2.964	1.006	2.490	1.010	1.760	1.031	1.658	1.047	1.604	1.008	7.138
MAA-EGDMA	1.185	0.802	1.113	0.818	1.116	0.792	1.090	0.822	1.074	0.810	1.062	0.842
MAA-DCM	1.005	1.296	1.009	0.476	1.020	0.472	1.028	0.468	1.050	0.490	1.067	0.468
MAA-MeOH	2.230	0.340	2.067	0.342	1.950	0.346	1.959	0.344	1.899	0.344	1.743	0.344
EGDMA-DCM	1.016	0.942	1.019	0.890	1.020	0.994	1.021	0.910	1.024	0.953		
EGDMA-MeOH	1.173	0.546	1.124	0.657	1.110	0.452	1.089	0.464	1.077	0.452	1.069	0.448
CTS-CTS	103.986	0.256	108.024	0.256	118.607	0.256	122.036	0.256	132.917	0.256	144.347	0.256
EGDMA-EGDMA	12.247	0.242	6.465	0.242	5.301	0.242	4.365	0.242	3.431	0.242		
MAA-MAA	37.400	0.242	38.480	0.242	41.918	0.242	42.977	0.242	47.306	0.242	51.372	0.242

Table S5. The maximum RDF peaks, $g(r)$ max, distance at which the maximum occurs, $r_{(g(r)\max)}$, for specific interactions between atom i of cortisol and atom j of MAA and EGDMA within the CL9-60 modelled systems.

	CL9		CL18		CL24		CL30		CL42		CL60	
	$g(r)$ max	$r_{(g(r)\max)}$ (nm)	$g(r)$ max	$r_{(g(r)\max)}$ (nm)	$g(r)$ max	$r_{(g(r)\max)}$ (nm)	$g(r)$ max	$r_{(g(r)\max)}$ (nm)	$g(r)$ max	$r_{(g(r)\max)}$ (nm)	$g(r)$ max	$r_{(g(r)\max)}$ (nm)
CTSO1-MAAH12	1.028	1.582	1.013	1.590	1.013	1.560	1.099	0.758	1.014	1.166	1.034	1.586
CTSH2-MAAO5	1.044	1.284	1.026	1.584	1.027	1.244	1.066	1.254	1.030	1.258	1.025	1.572
CTSH3-MAAO5	1.047	1.490	1.022	1.408	1.023	1.540	1.160	0.228	1.023	1.460	1.074	0.214
CTSO4-MAAH12	1.031	1.576	1.022	1.536	1.016	1.488	1.039	1.088	1.009	1.580	1.029	1.586
CTSH5-MAAO5	1.047	1.490	1.014	1.520	1.004	1.544	1.031	1.530	1.540	1.005	1.030	1.582
CTSH2-EGDMAO1	1.033	1.176	1.028	1.188	1.036	1.142	1.031	1.150	1.040	1.154	1.043	1.082
CTSH3-EGDMAO1	1.032	1.406	1.026	1.432	1.055	0.224	1.109	0.226	1.134	0.224	1.265	0.226
CTSH5-EGDMAO1	1.014	1.548	1.011	1.504	1.013	1.524	1.006	1.572	1.009	1.588	1.055	0.208

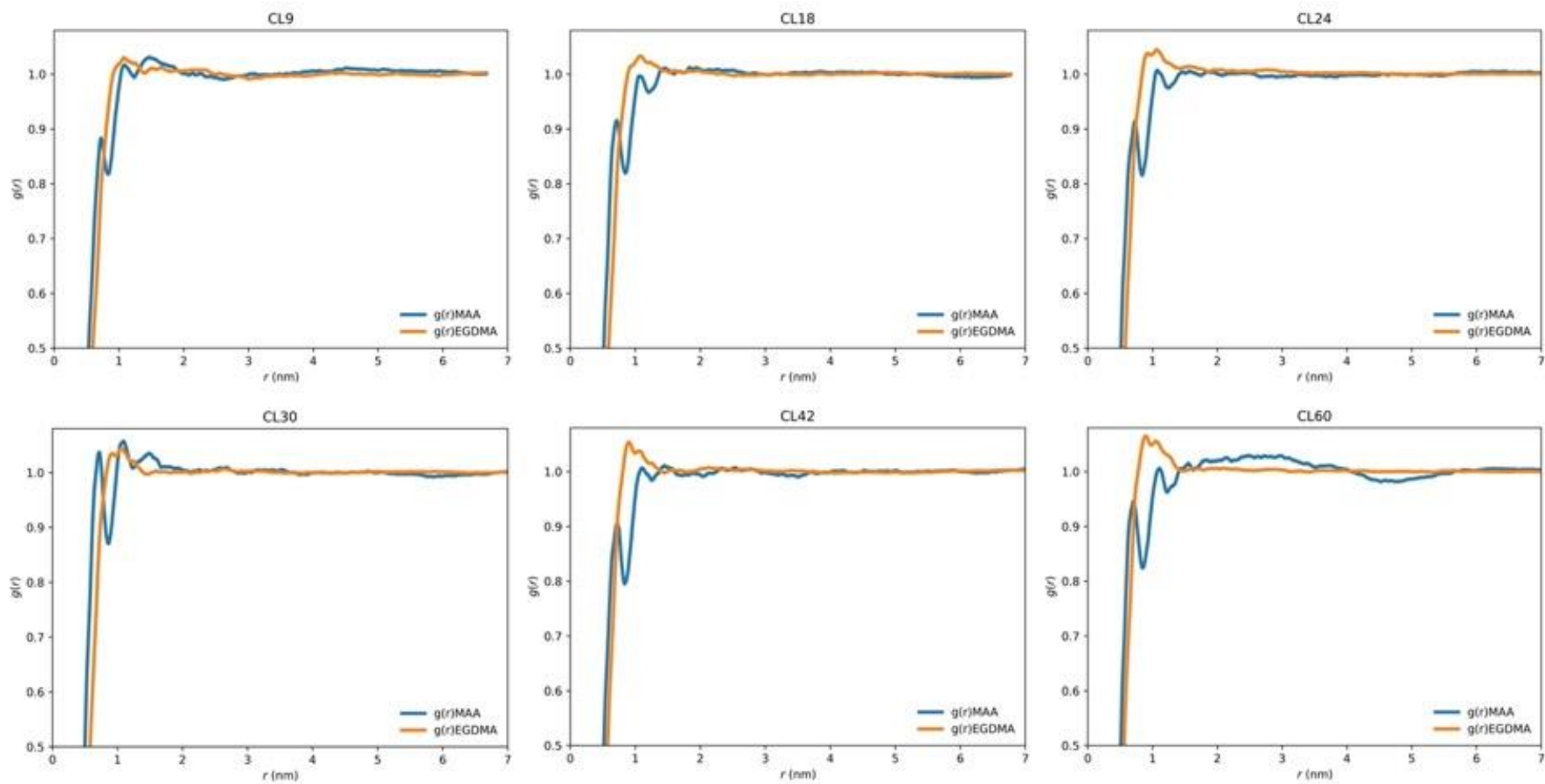
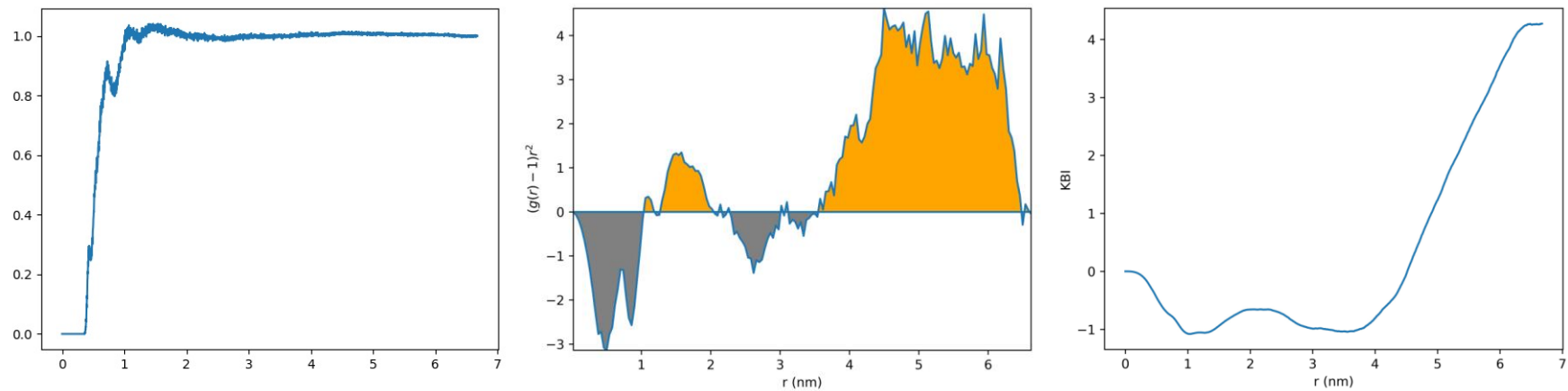


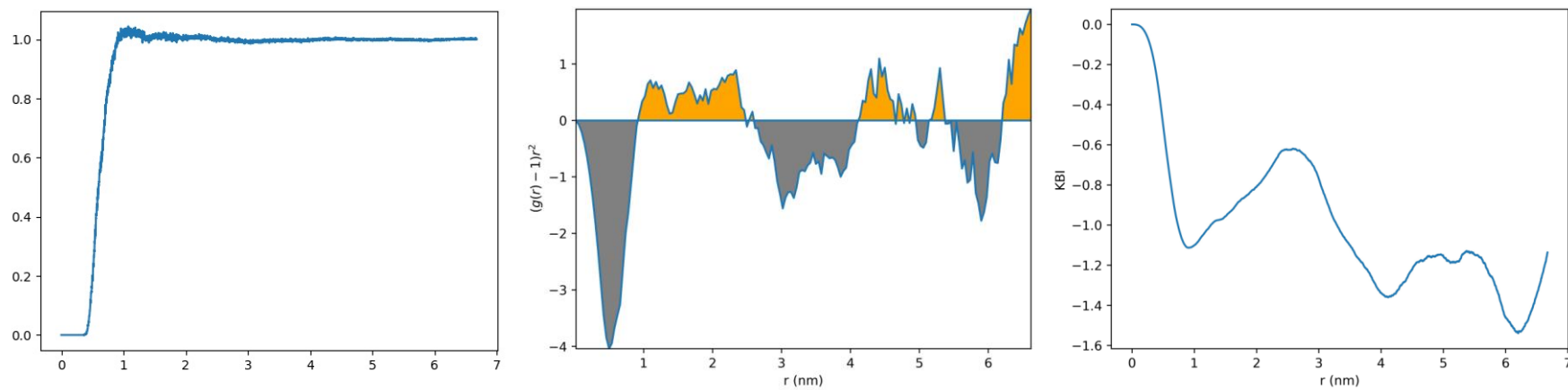
Figure S14. RDF comparison plots, $g(r)$ vs r between the centre of mass interactions MAA-CTS and EGDMA-CTS for each model system CL9-CL60.

The following plots **Figure S15(A-F)** include the RDF plot, $g(r)$ vs r , the repulsive (negative-grey) and attractive (positive-orange) regions $(g(r)-1)r^2$ vs r and the KBI vs r for the centre of mass (COM) interactions MAA-CTS and EGDMA-CTS for each model system CL9-CL60.

A
COM MAA CL9

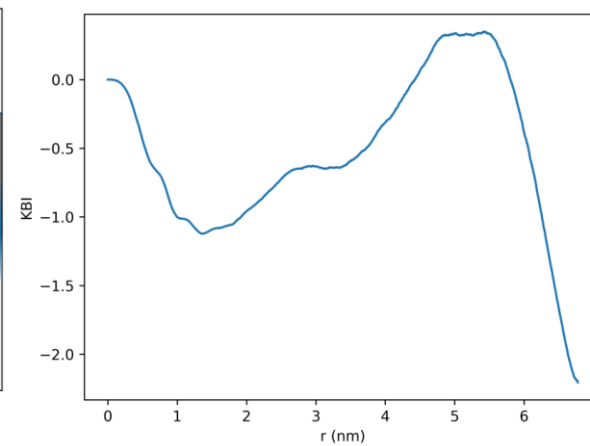
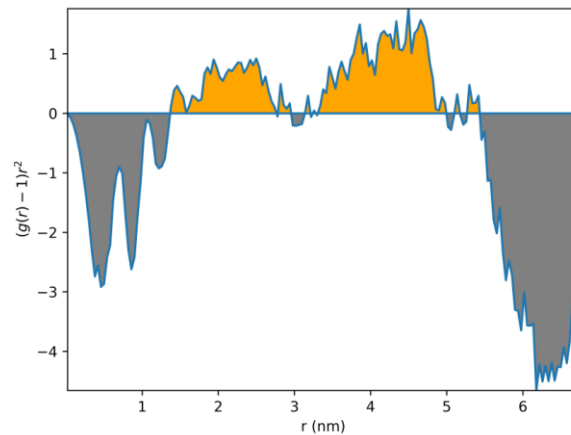
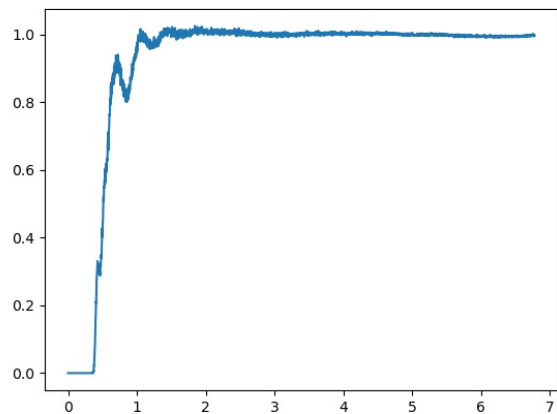


COM EGDMA CL9

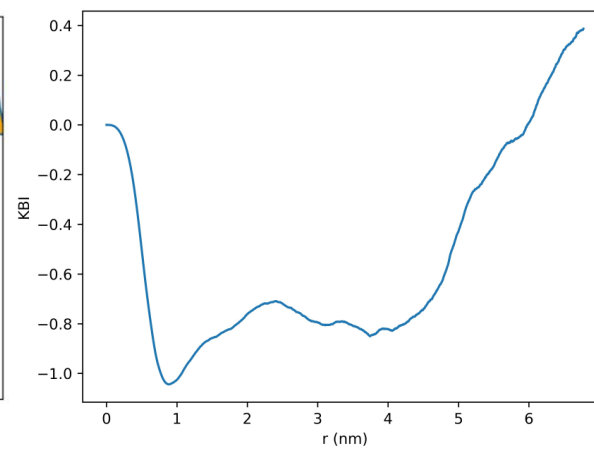
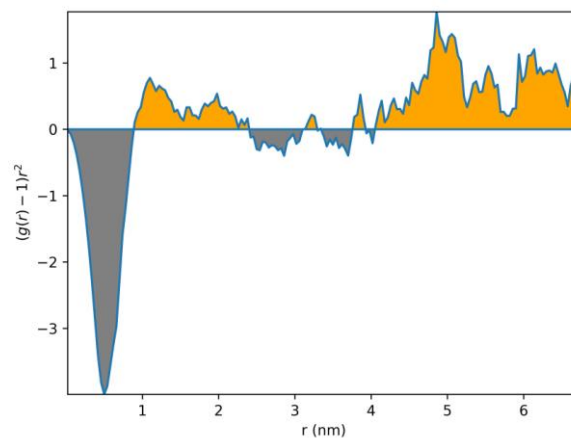
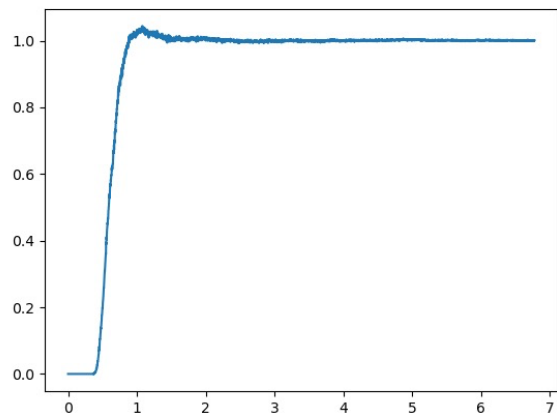


B

MAA CL18

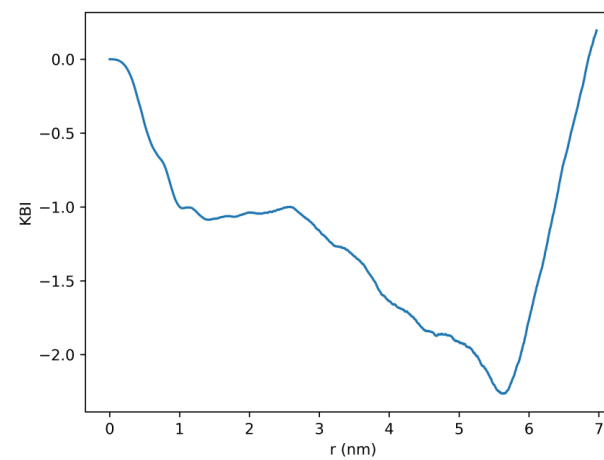
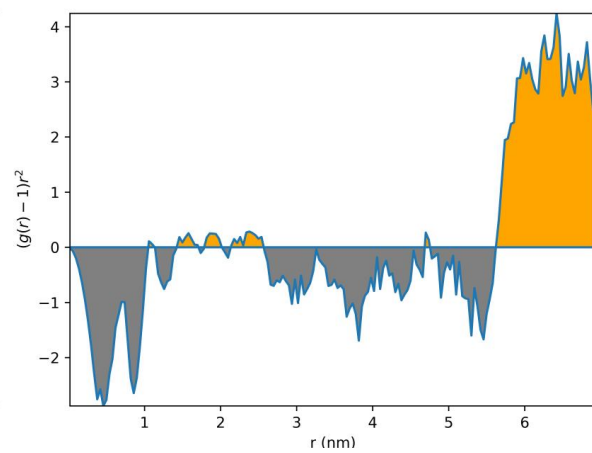
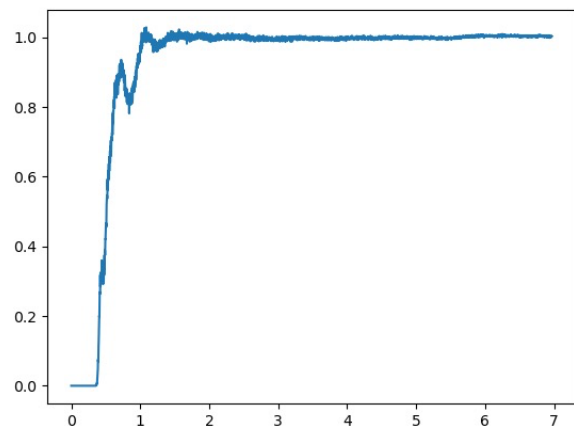


EGDMA CL18

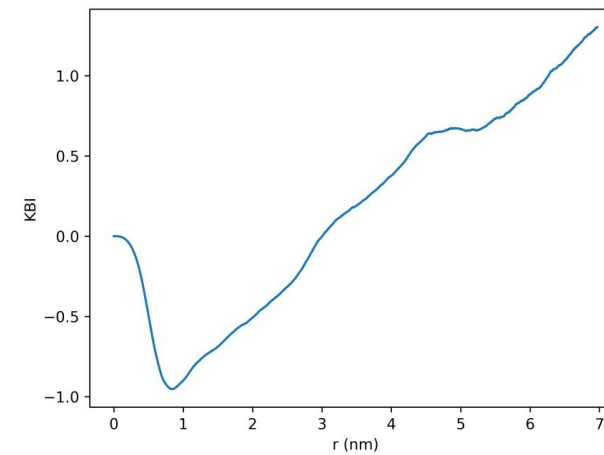
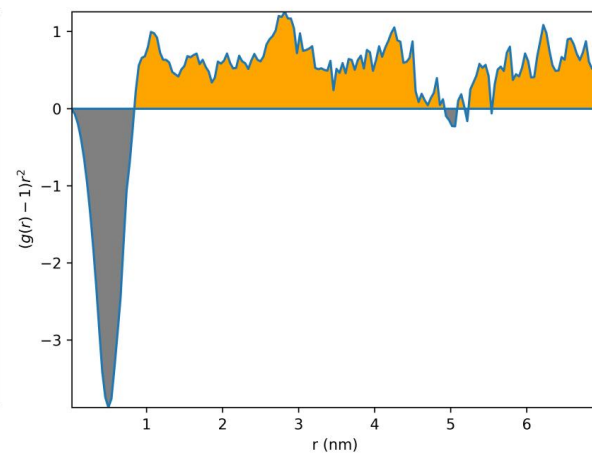
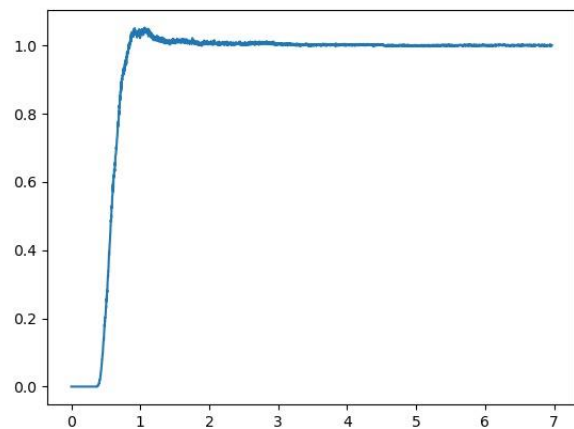


C

MAA CL24

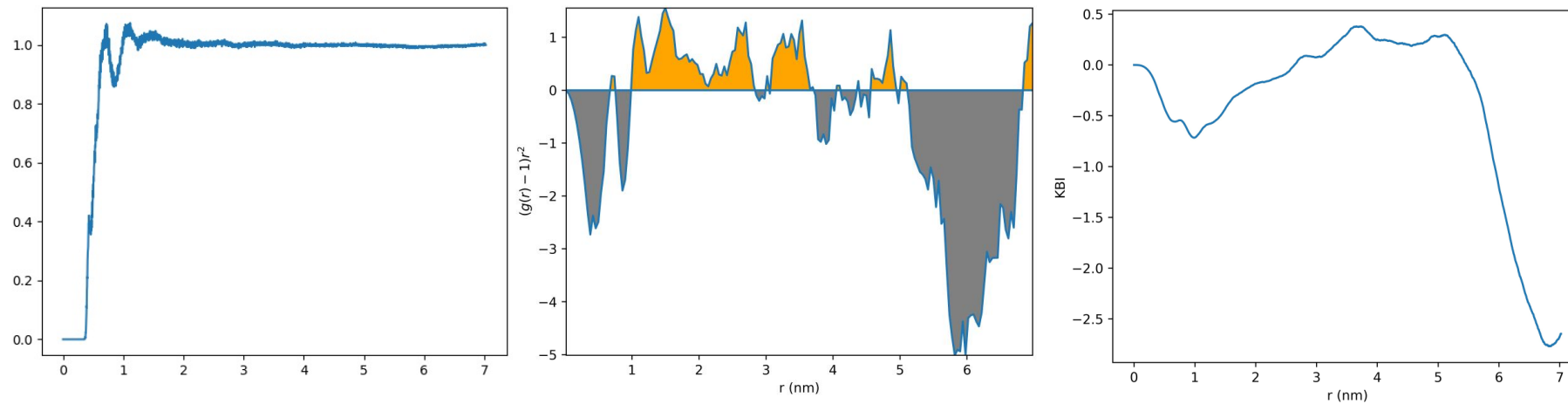


EGDMA CL24

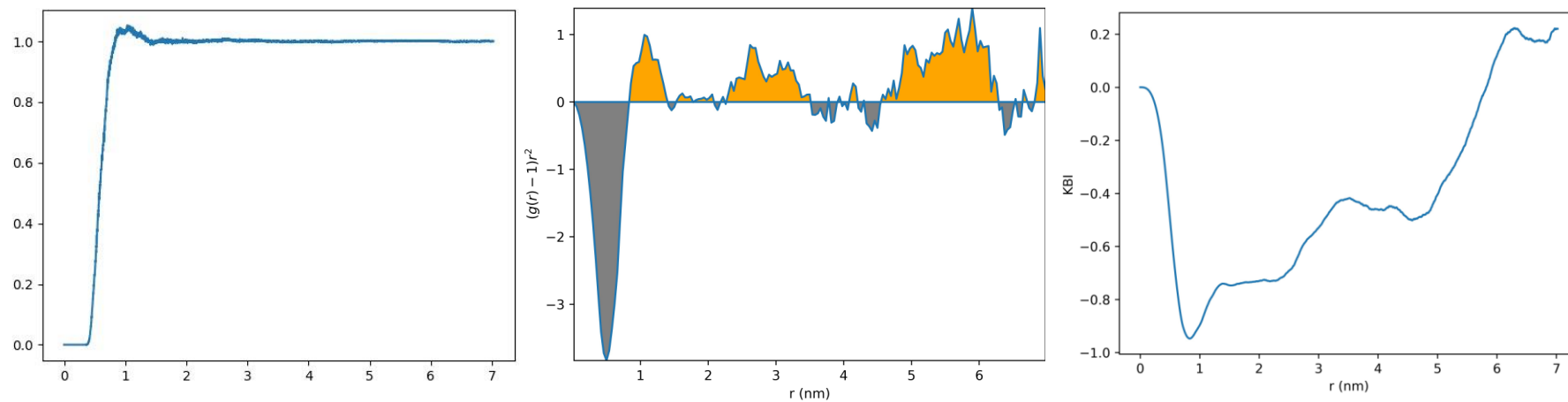


D

MAA CL30

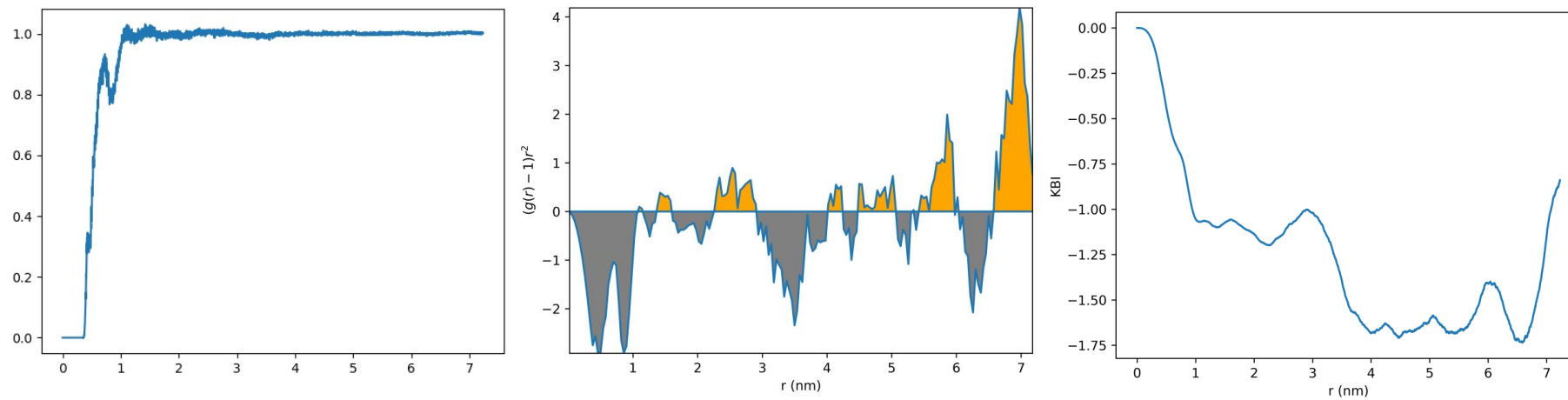


EGDMA CL30

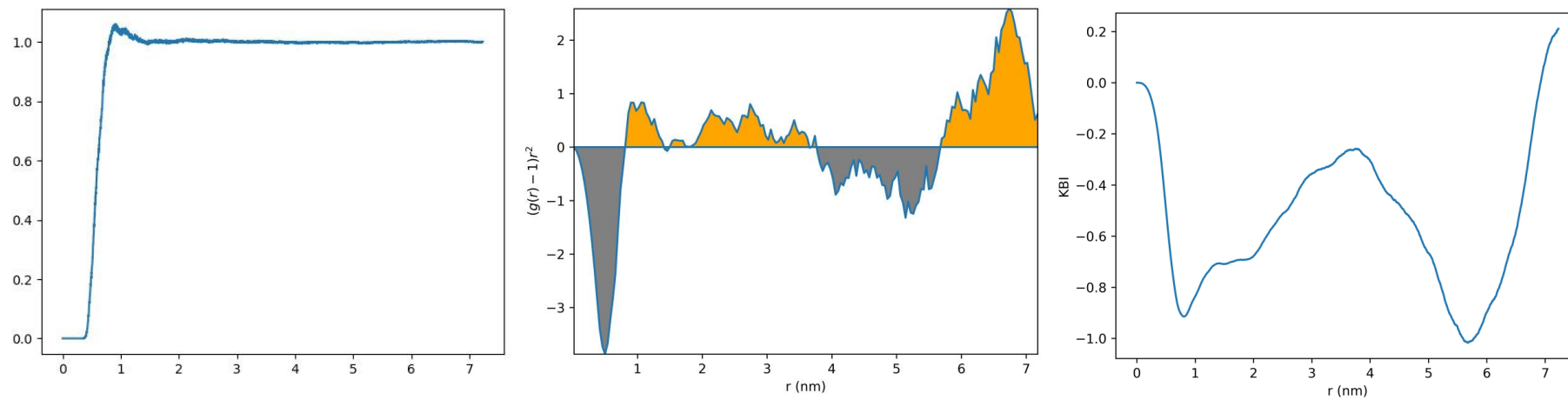


E

MAA CL42

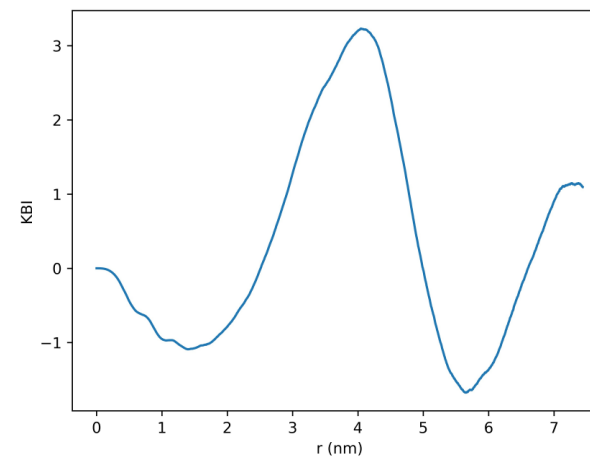
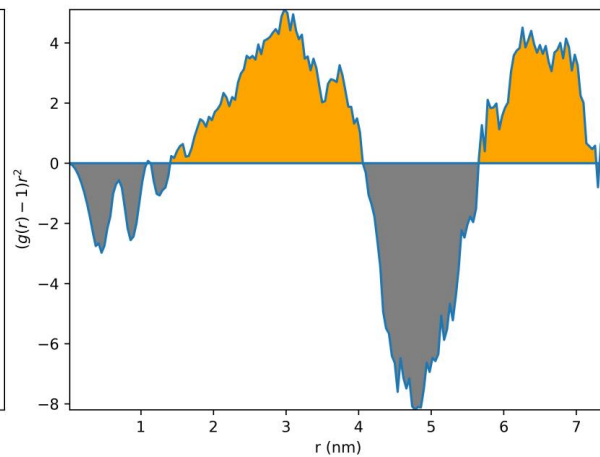
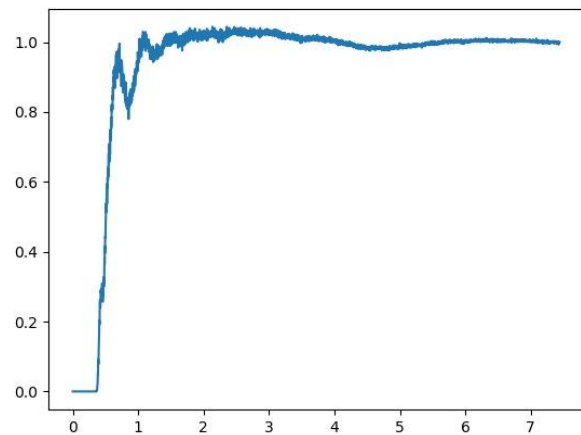


EGDMA CL42

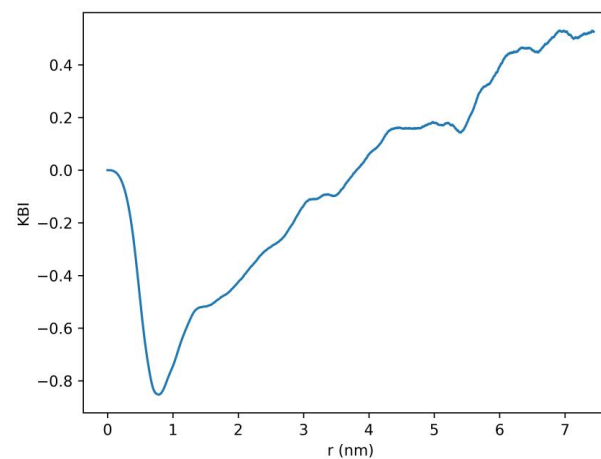
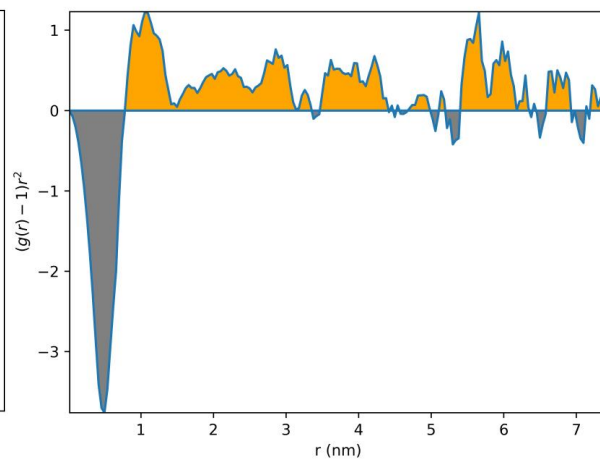
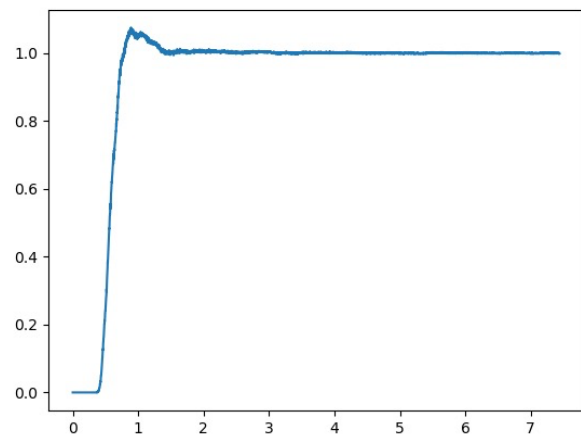


F

MAA CL60



EGDMA CL60



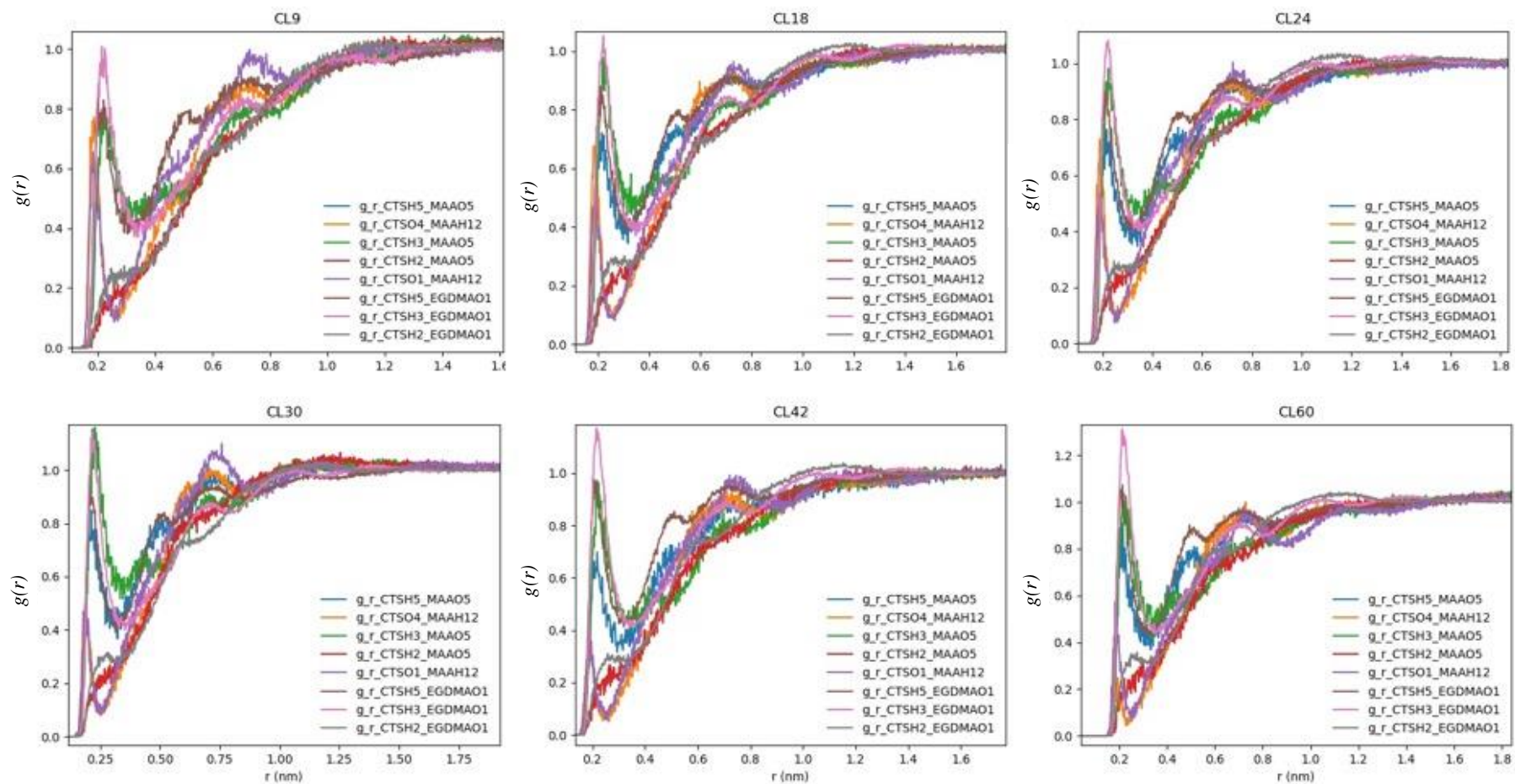


Figure S16. RDFs comparison plots between the atom pairs of MAA-CTS and EGDMA-CTS for each model system CL9-CL60.

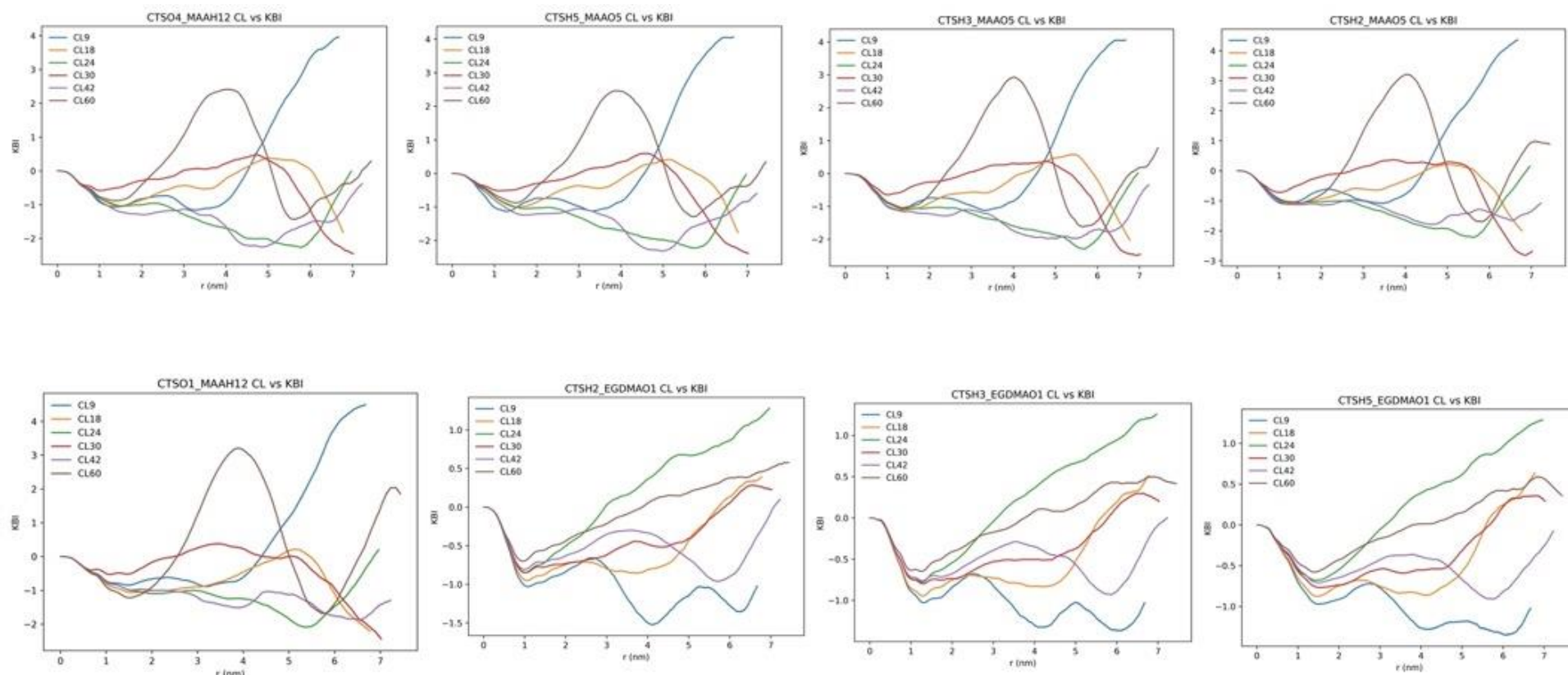
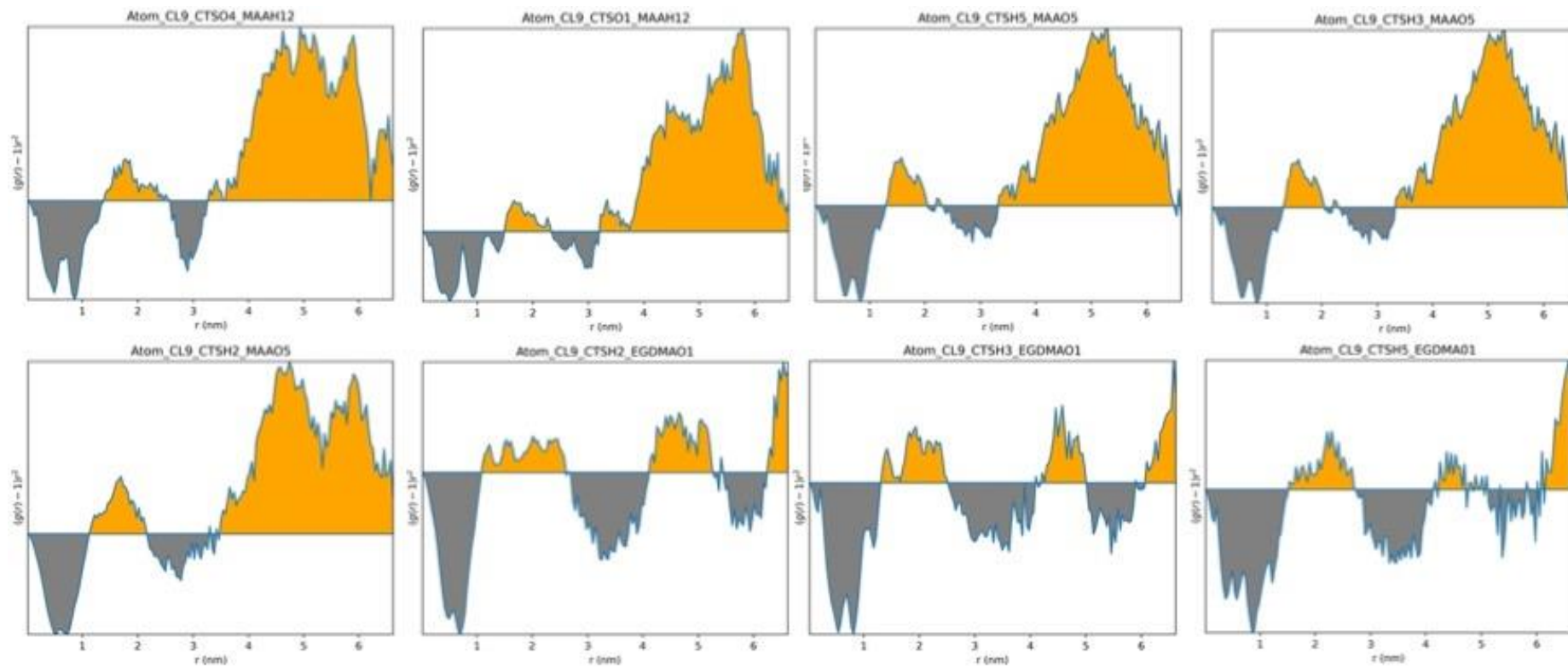
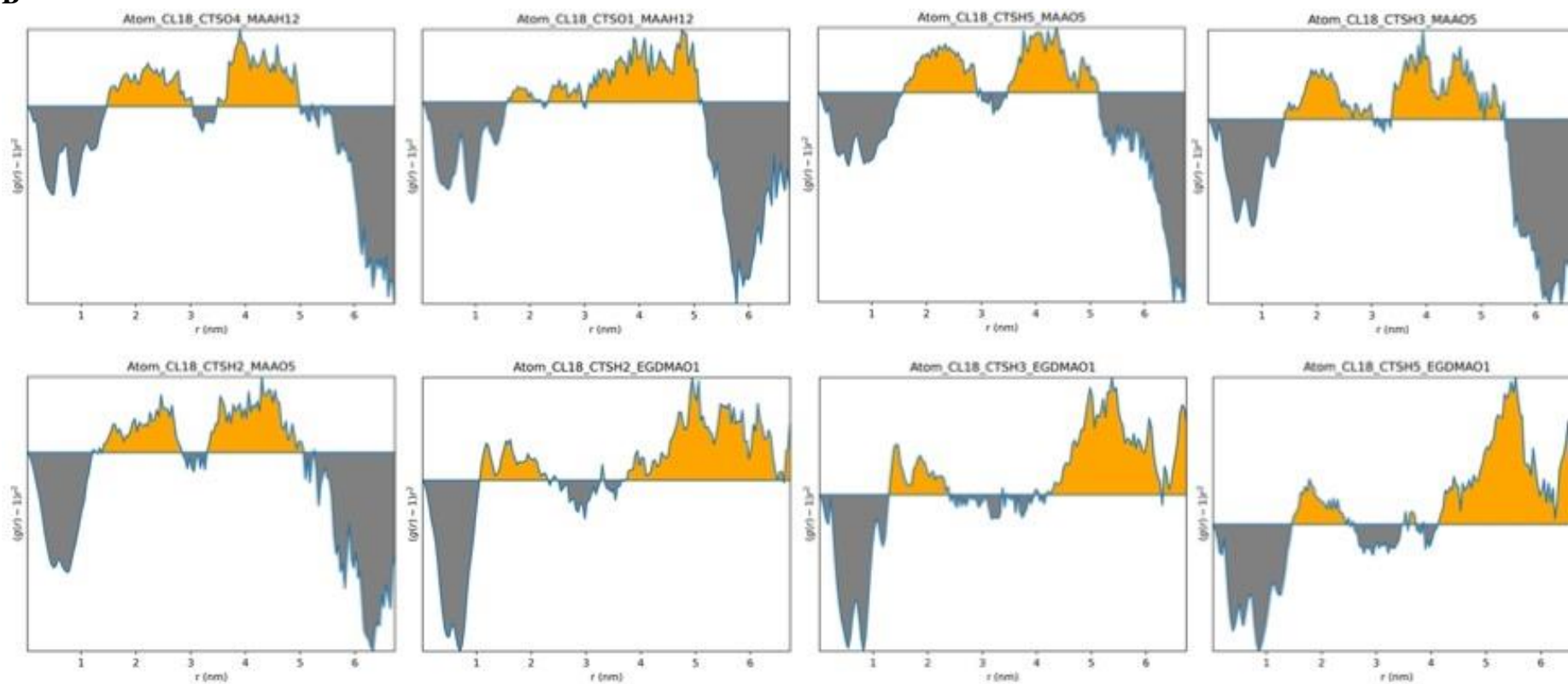


Figure S17. KBI comparison plots between the atom pairs of MAA-CTS and EGDMA-CTS for each model system CL9-CL60.

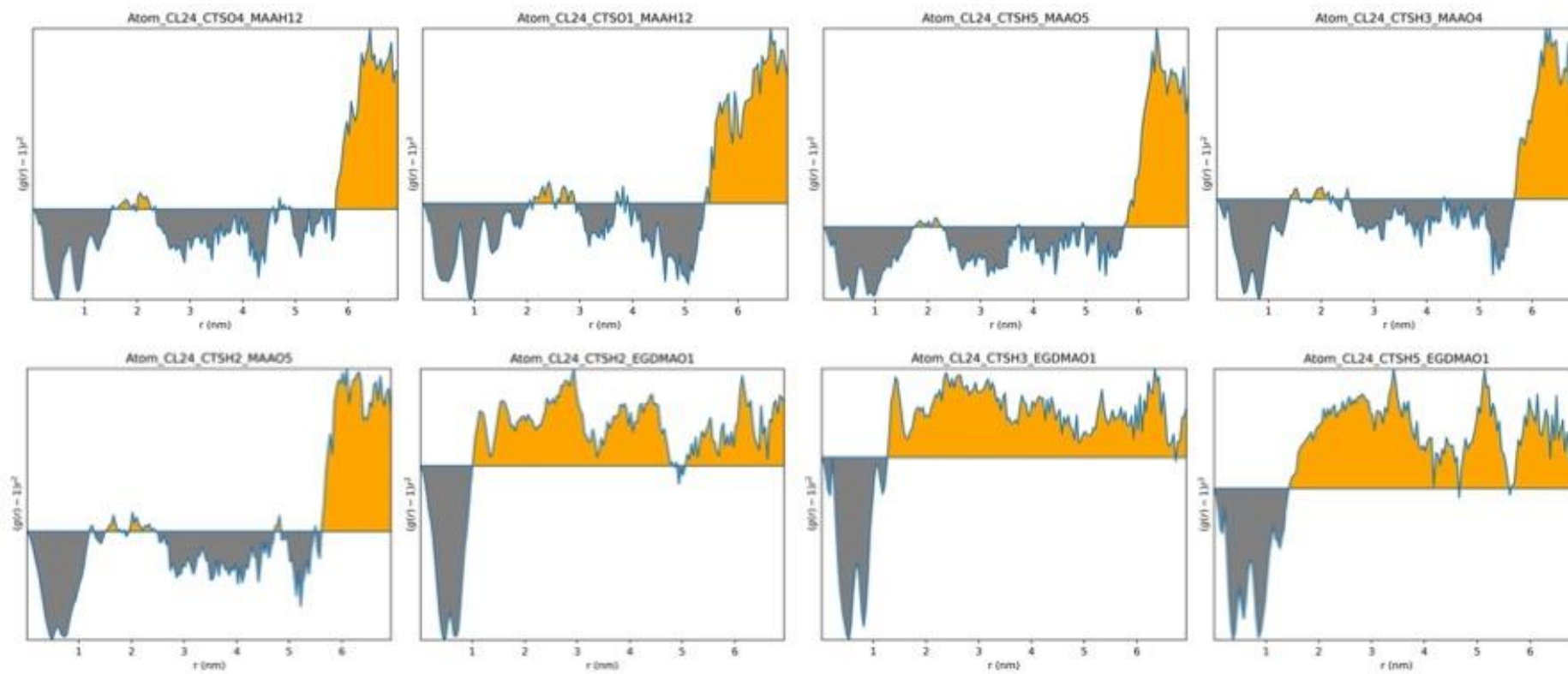
The following plots **Figure S18(A-F)**, include the repulsive (negative-grey) and attractive (positive-orange) filled regions $(g(r)-1)r^2$ vs r for the atom pairs labelled in **Figure 4** for MAA-CTS and EGDMA-CTS for each model system CL9-CL60.

A

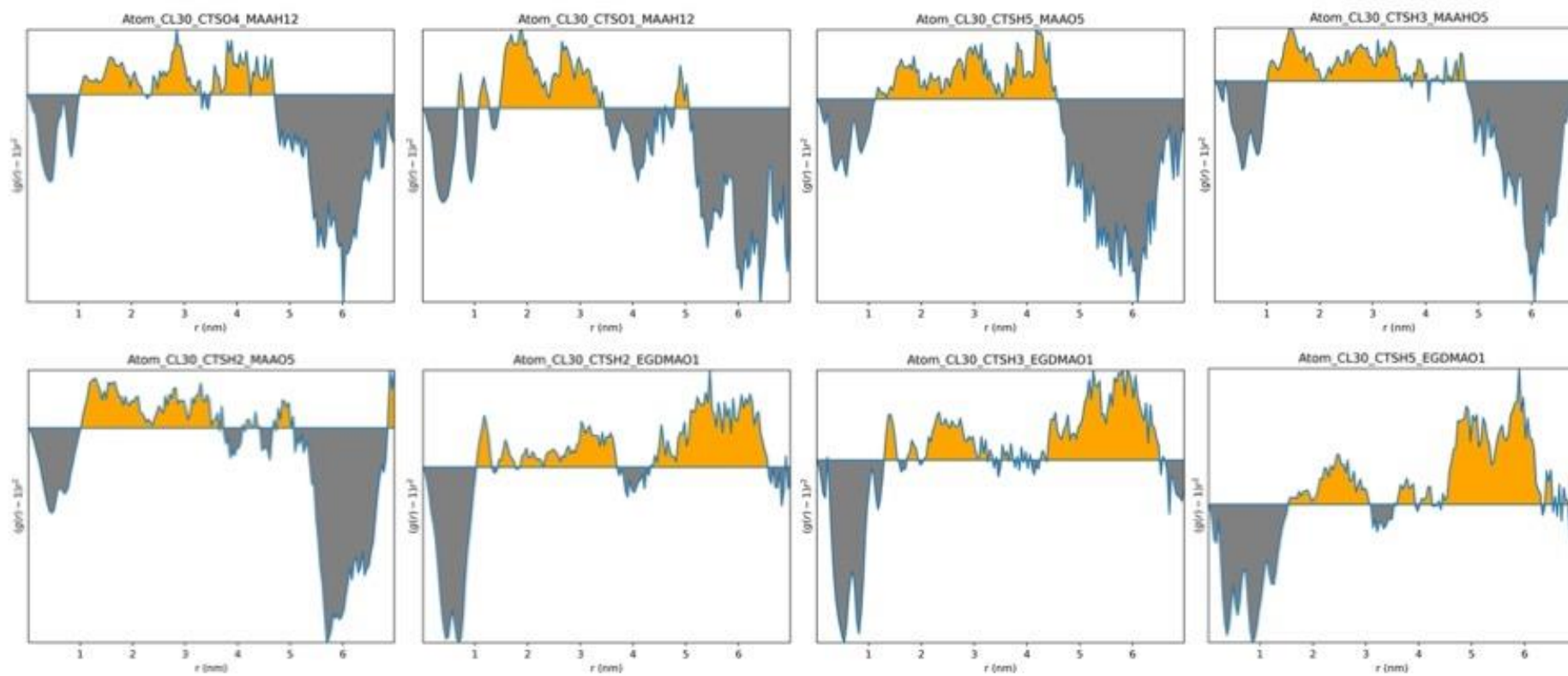


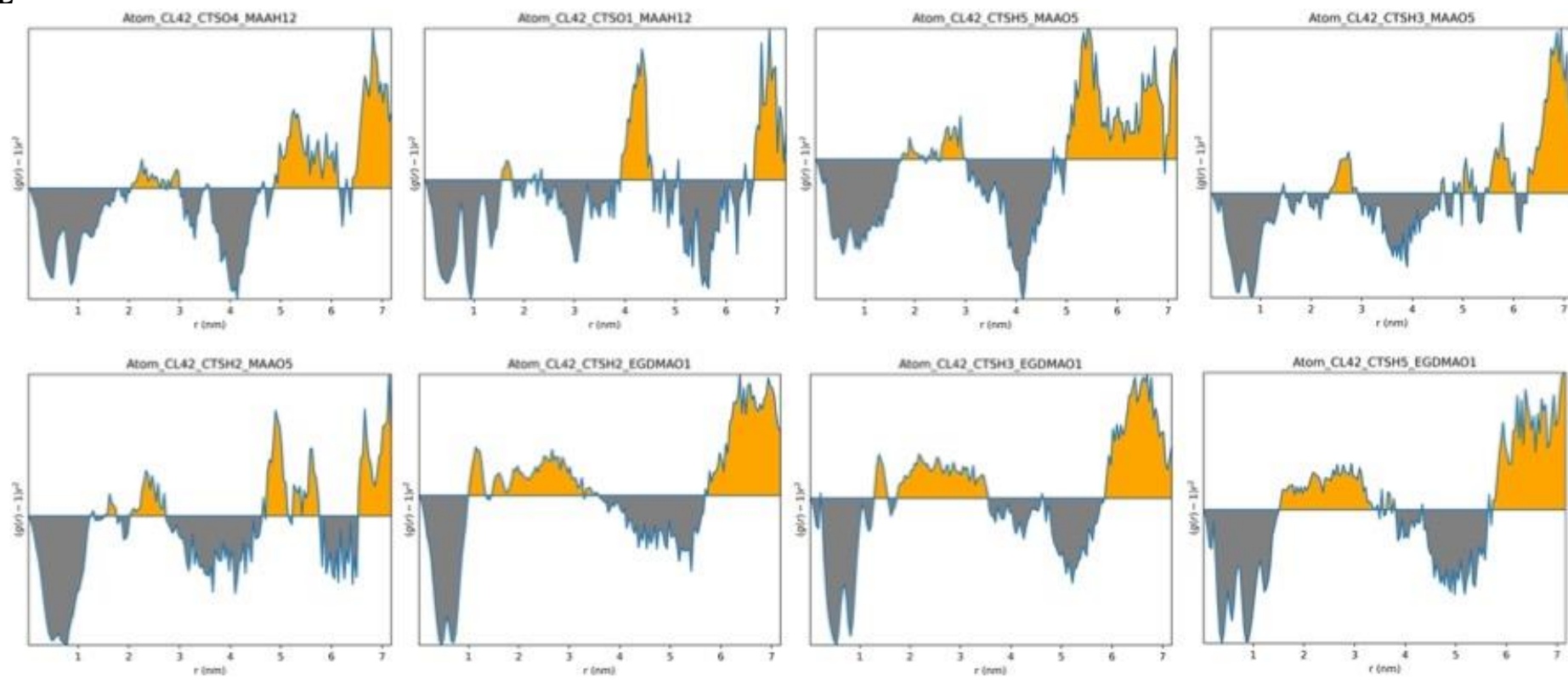
B

C



D



E

F